IEEJ Journal of Industry Applications
Vol.8 No.5 pp.745–755 DOI: 10.1541/ieejjia.8.745

Paper

Simplification of Motion Generation in the Singular Configuration of a Wheel-Legged Mobile Robot

Kenta Nagano[*a)] Member, Yasutaka Fujimoto[*] Senior Member

(Manuscript received May 1, 2018, revised Feb. 13, 2019)

Wheel-legged mobile robots (i.e., robots that use leg and wheel mechanisms) have the potential for efficient movement in response to the environment. Singular configuration is an inevitable problem in wheel-legged mobile robots and must be solved to realize motion. This paper proposes a simplification of the motion generation method in the singular configuration of a wheel-legged mobile robot. The problem of inverse kinematic calculations in a wheel-legged mobile robot is first modeled, and a solution method is proposed using an extension of the constraints to the acceleration level and the redundancy of the robot. The singular configuration problem in the low-speed region is then solved using the Levenberg–Marquardt method. A simple decision method using a weighted matrix for the damping factor is also proposed. The method is then verified using a three-dimensional simulation and an experiment.

Keywords: wheel-legged mobile robot, inverse kinematic calculation, singular configuration, Levenberg–Marquardt method

1. Introduction

Mobile robots can be classified as either wheeled or legged. Currently, wheeled mobile robots have several applications because they can achieve statically stable motion. A leg mechanism enables a mobile robot to move over uneven terrain. The wheel-legged mobile robot has both leg and wheel mechanisms, thus allowing varying modes of movement by using the wheel mechanism on flat planes and the leg mechanism on uneven terrain. For independent motion in varying environments, the robot must selectively use the leg or wheel mechanism. In this study, a mobile robot control method is developed to achieve motion in different environments by effectively using a wheel-legged mechanism. The wheel-legged mobile robot has been mentioned in several related studies: for example, in extreme environments [(1)–(3)] and in human-to-human support environments [(4)–(6)].

The wheel-legged mobile robot allows environmentally adaptable motion. However, the multiple mechanisms complicate the robot's structure. A robot with such mechanisms cannot avoid the problem of singular configuration, a posture in which the robot is structurally unable to achieve motion in a particular direction. Inverse kinematic calculations cannot obtain a solution for singular configuration. Thus, the singular configuration problem must be solved to achieve efficient motion that is adaptable to varying environments. Previously proposed methods to solve the singular configuration problem are discussed in this section. They can be classified into five categories: 1) using a special mechanism [(7)(8)], 2) trajectory generation for singular configuration avoidance [(9)–(11)], 3) using the redundancy of the robot [(12)–(14)], 4) analytically deriving the inverse kinematic solution [(15)(16)], and 5) numerically calculating the inverse kinematic solution [(17)–(21)].

An analytical solution to avoid singular configuration in a wheel-legged mobile robot was proposed by Grand *et al.*; however, only the steering joint was addressed [(22)]. An *et al.* proposed an inverse kinematic solution by offsetting the rotational axes of the steering joint and the wheel [(23)]. Suzumura *et al.* described an inverse kinematic calculation by considering multiple kinematic constraints of a wheel-legged mobile robot and proposed a selection matrix [(24)]. However, the method proposed by Grand *et al.* was inconsistent with motion because the steering joint calculation was conducted separately, whereas An *et al.*'s method required that the structure be changed beforehand, and Suzumura *et al.*'s method did not consider motion in the direction specified by the selection matrix and thus led to decreased motion performance. To address these problems, Suzumura *et al.* proposed a method for calculating multiple kinematic constraints by inverse kinematics that considered priority and obtained the inverse kinematic solution of the steering joint by expanding the constraints to the acceleration level [(25)]. However, this method had a new singular configuration in the low-speed region. Thus, these methods are not suitable approaches. Trajectory generation considering the singular configuration is also not suitable for a robot working in an unknown environment. Therefore, inverse kinematics that consider priority and the extension of constraints to the acceleration level are explored in this study. The Levenberg–Marquardt (LM) method [(26)(27)] is applied, and a method for determining a damping factor based on the robot manipulability as a solution to the singular configuration problem at low speeds is proposed. Manipulability is one of the indices that quantify robot operability from a kinematic viewpoint [(28)]. A method for determining a damping factor by resolving the influence of the steering joint was proposed for the wheel-legged mobile robot [(29)]. This method obtains the influence of the focus joint by separating the

a) Correspondence to: Kenta Nagano. E-mail: k.nagano@ieee.org
[*] Faculty of Engineering, Yokohama National University
79-5, Tokiwadai, Hodogaya-ku, Yokohama, Kanagawa 240-8501, Japan

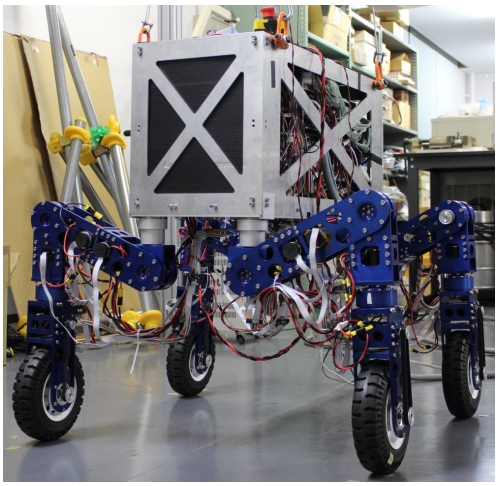

Fig. 1. Overview of the wheel-legged robot

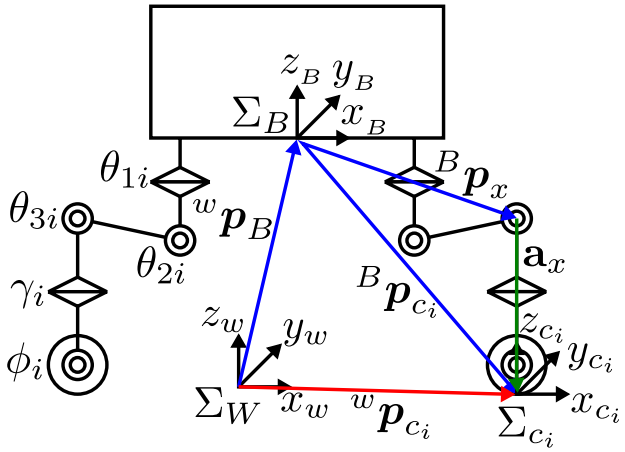

Fig. 2. Planar robot model in the sagittal plane

manipulability of the robot. In contrast, we propose a simpler method to realize the same effect as the previously reported conventional method.

This paper is organized as follows. The modeling and the problems of the inverse kinematic calculation in the wheel-legged mobile robot are described in Sect. 2. Section 3 presents a solution method for the problem of the inverse kinematic calculation using inverse kinematics that consider priority and the extension of constraints to the acceleration level. Section 4 then describes the singular configuration problem in the low-speed region and the application of the LM method to the wheel-legged mobile robot. Finally, the three-dimensional simulation and experiment performed to verify the efficacy of the proposed method are presented in Sect. 5, and the conclusions are drawn in Sect. 6.

2. Robot Modeling

2.1 Model and Coordinate Systems of the Robot

The coordinate systems of the wheel-legged mobile robot shown in Fig. 1 are defined as follows:

- Σ_W : coordinates of the world;
- Σ_B : coordinates of the base link; and
- Σ_{c_i} : coordinates of the contact point of the i^{th} wheel.

The planar robot model in the sagittal plane is shown in Fig. 2. In this model, ${}^w\boldsymbol{p}_B$, ${}^B\boldsymbol{p}_{c_i} \in \mathbb{R}^{3\times1}$ are the base position vectors with respect to Σ_W and the tip position vectors of each leg with respect to Σ_B. The index of each leg, i, is represented as $i = 1, \cdots, k$, where k is the total number of legs ($k = 4$ in the studied robot). Furthermore, $\boldsymbol{\Phi} = [\phi\ \theta\ \psi]^T$ is the Euler attitude angle of the base link and $\boldsymbol{\theta}_{legi} = [\theta_{1i}\ \theta_{2i}\ \theta_{3i}]^T \in \mathbb{R}^N$ is the joint angle vector of each leg, where N is the number of rotation joints in the leg ($N = 3$ in the studied robot). The crotch yaw, crotch roll, and knee roll joint rotation angle are θ_{1i}, θ_{2i}, and θ_{3i}, respectively, $\boldsymbol{\theta}_{wheeli} = [\gamma_i\ \phi_i]^T$ is the rotation angle related to wheeled locomotion, γ_i is the steering angle, and ϕ_i is the rolling angle of the wheel. Finally, the respective rotation information of each leg is summarized by $\boldsymbol{\theta}_i = [\boldsymbol{\theta}_{legi}^T\ \boldsymbol{\theta}_{wheeli}^T]^T$.

2.2 Kinematic Constraints on the Velocity Level

Both the mechanical and kinematic constraints, as well as the constraints for the leg and wheel mechanisms, must be considered for performing motion generation.

The kinematic constraints at the wheel contact point formulate as a nonslippage condition. Slippage of the contact point in the three-dimensional model was obtained from Grand *et al.* [22] and Suzumura and Fujimoto [25]:

$$\boldsymbol{v}_{s_i} = {}^w\dot{\boldsymbol{p}}_{c_i} - {}^w\boldsymbol{R}_{c_i}\begin{bmatrix} R\dot{\phi}_i \\ 0 \\ 0 \end{bmatrix} \cdots\cdots (1)$$

where $\boldsymbol{v}_{s_i}$ is the contact point slippage with respect to the coordinate system of the contact point of the i^{th} leg, R is the radius of the wheel, and ${}^w\boldsymbol{R}_{c_i}$ is a rotation matrix from Σ_w to Σ_{c_i}. The tip velocity vector of each leg with respect to Σ_w was then obtained by differentiating the tip position vector of each leg ${}^w\boldsymbol{p}_{c_i} = {}^w\boldsymbol{p}_B + {}^w\boldsymbol{R}_B{}^B\boldsymbol{p}_{c_i}$:

$${}^w\dot{\boldsymbol{p}}_{c_i} = {}^w\dot{\boldsymbol{p}}_B + {}^w\dot{\boldsymbol{R}}_B{}^B\boldsymbol{p}_{c_i} + {}^w\boldsymbol{R}_B{}^B\dot{\boldsymbol{p}}_{c_i} \cdots\cdots (2)$$

where ${}^w\dot{\boldsymbol{R}}_B$ is expressed as ${}^w\dot{\boldsymbol{R}}_B = {}^w\boldsymbol{\omega}_B{}^\wedge \cdot {}^w\boldsymbol{R}_B$. Furthermore, $\wedge$ is represented as an operator that transforms a 3×1 vector to a 3×3 skew-symmetric matrix, and the cross product can be rearranged into various forms: for example, $\mathbf{a}(\in \mathbb{R}^3) \times \mathbf{b}(\in \mathbb{R}^3) = -\mathbf{b} \times \mathbf{a} = -\mathbf{b}^\wedge\mathbf{a} = \mathbf{a}^\wedge\mathbf{b}$. Therefore, the second term on the right-hand side of Eq. (2) was transformed to $-({}^w\boldsymbol{R}_B{}^B\boldsymbol{p}_{c_i})^\wedge \cdot {}^w\boldsymbol{\omega}_B$. Here $\boldsymbol{v}_{si}$ in Eq. (1) was set to $\mathbf{0}$ to prevent slippage. For simplification, both sides of Eq. (1) were then multiplied by ${}^w\boldsymbol{R}_B^T$, transforming Eq. (1) into matrix form:

$$\mathbf{0} = \begin{bmatrix} {}^w\boldsymbol{R}_B^T & -{}^B\boldsymbol{p}_{c_i}^\wedge \end{bmatrix}\begin{bmatrix} {}^w\dot{\boldsymbol{p}}_B \\ {}^w\boldsymbol{\omega}_B \end{bmatrix} + \begin{bmatrix} \boldsymbol{J}_{legi} & \boldsymbol{J}_{\gamma_i} & -{}^B\boldsymbol{R}_{c_i}\begin{bmatrix} R \\ 0 \\ 0 \end{bmatrix} \end{bmatrix}\begin{bmatrix} \dot{\boldsymbol{\theta}}_{legi} \\ \dot{\gamma}_i \\ \dot{\phi}_i \end{bmatrix} \cdots\cdots (3)$$

$$= \boldsymbol{J}_{B_i}\boldsymbol{\xi}_{B_i} + \boldsymbol{J}_{W_i}^{vel}\dot{\boldsymbol{\theta}}_i \cdots\cdots (4)$$

where $\boldsymbol{J}_{legi} \in \mathbb{R}^{N\times N}$ is the Jacobian matrix of the rotational joint of the i^{th} leg, and $\boldsymbol{J}_{\gamma_i} \in \mathbb{R}^{3\times1}$ is the Jacobian matrix of the steering joint. Each Jacobian matrix can be obtained by the cross product of the rotational axis vector $\mathbf{z}_x$ and the vector connecting each joint center to the corresponding leg contact point, $\mathbf{a}_x (= {}^B\boldsymbol{p}_{c_i} - {}^B\boldsymbol{p}_x)$. From Eq. (3), the entire body motion satisfying the nonslippage constraints at the wheel contact point can be generated.

However, the tip position control cannot be uniquely determined by constraints at the wheel contact point because the

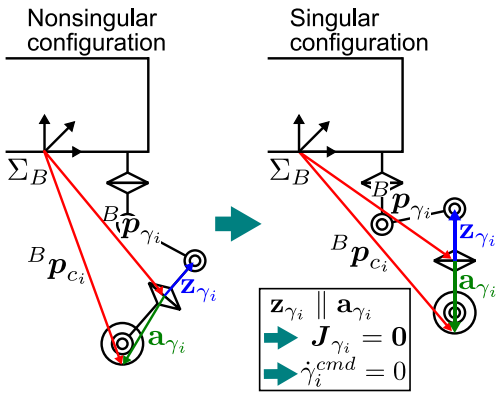

Fig. 3. Singular configuration of the steering joint

solution of the various combinations of $\begin{bmatrix}\dot{\boldsymbol{\theta}}_{legi} & \dot{\gamma}_i & \dot{\phi}_i\end{bmatrix}^T$ occurs. Therefore, the leg position constraint was given by the tip velocity vector of each leg with respect to Σ_B, expressed as

$$ {}^B\dot{\boldsymbol{p}}_{c_i} = \begin{bmatrix}\boldsymbol{J}_{legi} & \boldsymbol{J}_{\gamma_i} & \mathbf{0}\end{bmatrix}\begin{bmatrix}\dot{\boldsymbol{\theta}}_{legi}\\ \dot{\gamma}_i\\ \dot{\phi}_i\end{bmatrix} \cdots\cdots (5) $$

$$ = \boldsymbol{J}_{L_i}^{vel}\dot{\boldsymbol{\theta}}_i \cdots\cdots (6) $$

where $\boldsymbol{J}_{L_i}^{vel} \in \mathbb{R}^{3\times(N+2)}$. Thus, the contact point position for each leg can be controlled by the leg position constraints.

2.3 Problems in the Inverse Kinematic Calculation

Here, the problems of the inverse kinematic calculation are described by the kinematic constraints on the velocity level. First, the coefficient matrix $\boldsymbol{J}_{\gamma_i}$ becomes equal to $\mathbf{0}$ when the vector $\mathbf{a}_{\gamma_i}(= {}^B\boldsymbol{p}_{c_i} - {}^B\boldsymbol{p}_{\gamma_i})$ and the rotation axis vector $\mathbf{z}_{\gamma_i}$ are coaxial in the cross product calculation. Therefore, the wheel-legged mobile robot cannot generate appropriate steering with a turning motion; this singular configuration of the steering joint is shown in Fig. 3. Another problem in the inverse kinematic calculation occurs when the constraints of the wheel and leg positions are simultaneously solved. Eqs. (3) and (5) are combined when these are simultaneously solved:

$$ \begin{bmatrix}\mathbf{0}\\ {}^B\dot{\boldsymbol{p}}_{c_i}\end{bmatrix} = \begin{bmatrix}{}^w\boldsymbol{R}_B^T & -{}^B\boldsymbol{p}_{c_i}^{\wedge}\\ \mathbf{0} & \mathbf{0}\end{bmatrix}\begin{bmatrix}{}^w\dot{\boldsymbol{p}}_B\\ {}^w\boldsymbol{\omega}_B\end{bmatrix} + \begin{bmatrix}\boldsymbol{J}_{legi} & \boldsymbol{J}_{\gamma_i} & -{}^B\boldsymbol{R}_{c_i}\begin{bmatrix}R\\0\\0\end{bmatrix}\\ \boldsymbol{J}_{legi} & \boldsymbol{J}_{\gamma_i} & \mathbf{0}\end{bmatrix}\begin{bmatrix}\dot{\boldsymbol{\theta}}_{legi}\\ \dot{\gamma}_i\\ \dot{\phi}_i\end{bmatrix} \cdots\cdots (7) $$

The pseudo-inverse matrix of the coefficient matrix in the second term on the right-hand side of Eq. (7) is necessary for the inverse kinematic calculation. The size of the coefficient matrix is $6 \times (N + 2)$. Thus, the rank r must be $N + 2$ when calculating the pseudo-inverse matrix ($N = 3$ and $r = 5$ in the studied robot). The rank of the coefficient matrix is given as

$$ r = \mathrm{rank}\left(\begin{bmatrix}\boldsymbol{J}_{legi} & \boldsymbol{J}_{\gamma_i} & -{}^B\boldsymbol{R}_{c_i}\begin{bmatrix}R\\0\\0\end{bmatrix}\\ \boldsymbol{J}_{legi} & \boldsymbol{J}_{\gamma_i} & \mathbf{0}\end{bmatrix}\right) \cdots\cdots (8) $$

Then, Eq. (8) is transformed by the elementary transformation of the matrix as follows:

$$ r = \mathrm{rank}\left(\begin{bmatrix}\mathbf{0} & \mathbf{0} & -{}^B\boldsymbol{R}_{c_i}\begin{bmatrix}R\\0\\0\end{bmatrix}\\ \boldsymbol{J}_{legi} & \boldsymbol{J}_{\gamma_i} & \mathbf{0}\end{bmatrix}\right) \cdots\cdots (9) $$

$$ = \mathrm{rank}\left(\begin{bmatrix}\boldsymbol{J}_{legi} & \boldsymbol{J}_{\gamma_i}\end{bmatrix}\right) + \mathrm{rank}\left(-{}^B\boldsymbol{R}_{c_i}\begin{bmatrix}R\\0\\0\end{bmatrix}\right) \cdots\cdots (10) $$

From Eq. (10), the ranks of the first term and the second term on the right side are less than 3 and 1, respectively. Therefore, the rank of the coefficient matrix becomes $r \leq 4$. From this result, the inverse kinematic solution cannot be obtained because the pseudo-inverse matrix is not appropriate due to the rank deficiency.

3. Method Using Redundancy in the Acceleration Level

In this section, the singular configuration problem is solved for the velocity level of the steering joint by extending the kinematic constraints to the acceleration level. A method of solving the inverse kinematics considering priority for problems with simultaneous constraints is also discussed [25].

3.1 Kinematic Constraints on the Acceleration Level

The wheel constraints on the acceleration level were obtained by differentiating Eq. (3) with respect to time:

$$ \begin{aligned}\mathbf{0} = {}&{}^w\boldsymbol{R}_B^T{}^w\ddot{\boldsymbol{p}}_B + {}^w\dot{\boldsymbol{R}}_B^T{}^w\dot{\boldsymbol{p}}_B - {}^B\dot{\boldsymbol{p}}_{c_i} \times {}^w\boldsymbol{\omega}_B - {}^B\boldsymbol{p}_{c_i} \times {}^w\dot{\boldsymbol{\omega}}_B\\ &+\boldsymbol{J}_{legi}\ddot{\boldsymbol{\theta}}_{legi} + \boldsymbol{J}_{\gamma_i}\ddot{\gamma}_i + \dot{\boldsymbol{J}}_{legi}\dot{\boldsymbol{\theta}}_{legi} + \dot{\boldsymbol{J}}_{\gamma_i}\dot{\gamma}_i\\ &-{}^B\dot{\boldsymbol{R}}_{c_i}\begin{bmatrix}R\dot{\phi}_i\\0\\0\end{bmatrix} - {}^B\boldsymbol{R}_{c_i}\begin{bmatrix}R\ddot{\phi}_i\\0\\0\end{bmatrix} \cdots\cdots (11)\end{aligned} $$

where ${}^w\dot{\boldsymbol{R}}_B^T$ and ${}^B\dot{\boldsymbol{R}}_{c_i}$ are expressed as ${}^w\dot{\boldsymbol{R}}_B^T = ({}^w\boldsymbol{\omega}_B^{\wedge}{}^w\boldsymbol{R}_B)^T$ and ${}^B\dot{\boldsymbol{R}}_{c_i} = {}^B\boldsymbol{\omega}_{c_i}^{\wedge}{}^B\boldsymbol{R}_{c_i}$, respectively. Furthermore, ${}^B\boldsymbol{\omega}_{c_i}$ was transformed as follows:

$$ {}^B\boldsymbol{\omega}_{c_i} = ({}^B\boldsymbol{\omega}_{\theta_{1i}} + \cdots + {}^B\boldsymbol{\omega}_{\theta_{Ni}}) + {}^B\boldsymbol{\omega}_{\gamma_i} \cdots\cdots (12) $$

$$ = (\mathbf{z}_{\theta_{1i}}\dot{\theta}_{1i} + \cdots + \mathbf{z}_{\theta_{Ni}}\dot{\theta}_{Ni}) + \mathbf{z}_{\gamma_i}\dot{\gamma}_i \cdots\cdots (13) $$

$$ = \boldsymbol{J}_{legi}^{\omega}\dot{\boldsymbol{\theta}}_{legi} + \boldsymbol{J}_{\gamma_i}^{\omega}\dot{\gamma}_i \cdots\cdots (14) $$

where $\boldsymbol{J}_{legi}^{\omega} = \begin{bmatrix}\mathbf{z}_{\theta_{1i}} & \cdots & \mathbf{z}_{\theta_{Ni}}\end{bmatrix} \in \mathbb{R}^{3\times N}$, $\boldsymbol{J}_{\gamma_i}^{\omega} = \mathbf{z}_{\gamma_i} \in \mathbb{R}^3$. Then, ${}^B\boldsymbol{\omega}_{c_i}^{\wedge}$ was obtained as $(\boldsymbol{J}_{legi}^{\omega}\dot{\boldsymbol{\theta}}_{legi})^{\wedge} + \boldsymbol{J}_{\gamma_i}^{\omega\wedge}\dot{\gamma}_i$. Therefore, Eq. (11) can be expressed in matrix form:

$$ \begin{aligned}\mathbf{0} = {}&\begin{bmatrix}{}^w\boldsymbol{R}_B^T & -{}^B\boldsymbol{p}_{c_i}^{\wedge}\end{bmatrix}\begin{bmatrix}{}^w\ddot{\boldsymbol{p}}_B\\ {}^w\dot{\boldsymbol{\omega}}_B\end{bmatrix}\\ &+\begin{bmatrix}\boldsymbol{J}_{legi} & \dot{\boldsymbol{J}}_{\gamma_i} + {}^w\boldsymbol{\omega}_B^{\wedge}\boldsymbol{J}_{\gamma_i} - \boldsymbol{J}_{\gamma_i}^{\omega\wedge}{}^B\boldsymbol{R}_{c_i}\begin{bmatrix}R\dot{\phi}_i\\0\\0\end{bmatrix} & {}^B\boldsymbol{R}_{c_i}\begin{bmatrix}-R\\0\\0\end{bmatrix}\end{bmatrix}\begin{bmatrix}\ddot{\boldsymbol{\theta}}_{legi}\\ \ddot{\gamma}_i\\ \ddot{\phi}_i\end{bmatrix}\\ &+({}^w\boldsymbol{\omega}_B^{\wedge}{}^w\boldsymbol{R}_B)^T{}^w\dot{\boldsymbol{p}}_B + {}^w\boldsymbol{\omega}_B^{\wedge}\boldsymbol{J}_{legi}\dot{\boldsymbol{\theta}}_{legi} + \dot{\boldsymbol{J}}_{legi}\dot{\boldsymbol{\theta}}_{legi}\\ &+\boldsymbol{J}_{\gamma_i}\ddot{\gamma}_i - (\boldsymbol{J}_{legi}^{\omega}\dot{\boldsymbol{\theta}}_{legi})^{\wedge}{}^B\boldsymbol{R}_{c_i}\begin{bmatrix}R\dot{\phi}_i\\0\\0\end{bmatrix} \cdots\cdots (15)\\ = {}&\boldsymbol{J}_{B_i}\dot{\boldsymbol{\xi}}_B + \boldsymbol{J}_{W_i}^{acc}\boldsymbol{\eta}_i + \mathbf{b}_{W_i} \cdots\cdots (16)\end{aligned} $$

where $\boldsymbol{J}_{W_i}^{acc} \in \mathbb{R}^{3\times(N+2)}$, $\mathbf{b}_{W_i} \in \mathbb{R}^3$. $\boldsymbol{\eta}_i = \begin{bmatrix}\ddot{\boldsymbol{\theta}}_{legi} & \ddot{\gamma}_i & \ddot{\phi}_i\end{bmatrix}^T$ is a vector composed of the angular acceleration of the joints $\ddot{\boldsymbol{\theta}}_{legi}$ and wheel $\ddot{\phi}_i$ and the angular velocity of the steering

joint $\dot{\gamma}_i$. From the second column vector in the second term of the right-hand side of Eq. (15), this term does not become zero in the singular configuration of the steering joint because $-\boldsymbol{J}_{\gamma_i}^{\omega\wedge B}\boldsymbol{R}_{c_i}\begin{bmatrix}R\dot{\phi}_i & 0 & 0\end{bmatrix}^T$ has a value even if the steering rotation axis is perpendicular to the ground surface. Therefore, a steering joint motion can be obtained in the singular configuration.

Next, the constraints of the leg position on the acceleration level were obtained by differentiating Eq. (5) with respect to time and expressing it in matrix form:

$$
\begin{aligned}
{}^B\ddot{\boldsymbol{p}}_{c_i} &= \dot{\boldsymbol{J}}_{leg_i}\dot{\boldsymbol{\theta}}_{leg_i} + \boldsymbol{J}_{leg_i}\ddot{\boldsymbol{\theta}}_{leg_i} + \dot{\boldsymbol{J}}_{\gamma_i}\dot{\gamma}_i + \boldsymbol{J}_{\gamma_i}\ddot{\gamma}_i \cdots\cdots (17)\\
&= \begin{bmatrix}\boldsymbol{J}_{leg_i} & \dot{\boldsymbol{J}}_{\gamma_i} & 0\end{bmatrix}\begin{bmatrix}\ddot{\boldsymbol{\theta}}_{leg_i}\\ \dot{\gamma}_i\\ \ddot{\phi}_i\end{bmatrix} + \dot{\boldsymbol{J}}_{leg_i}\dot{\boldsymbol{\theta}}_{leg_i} + \boldsymbol{J}_{\gamma_i}\ddot{\gamma}_i \cdots\cdots (18)\\
&= \boldsymbol{J}_{L_i}^{acc}\boldsymbol{\eta}_i + \mathbf{b}_{Li} \cdots\cdots (19)
\end{aligned}
$$

where $\boldsymbol{J}_{L_i}^{acc} \in \mathbb{R}^{3\times(N+2)}$ and $\mathbf{b}_{L_i} \in \mathbb{R}^3$.

Kinematic constraints considering all the legs can be expressed from the leg position and wheel constraints on the acceleration level:

$$
\begin{bmatrix}\mathbf{0}\\ \mathbf{0}\\ \vdots\\ \mathbf{0}\end{bmatrix} = \begin{bmatrix}\boldsymbol{J}_{B_1}\\ \boldsymbol{J}_{B_2}\\ \vdots\\ \boldsymbol{J}_{B_k}\end{bmatrix}\dot{\boldsymbol{\xi}}_B + \begin{bmatrix}\boldsymbol{J}_{W_1}^{acc} & \mathbf{0} & \cdots & \mathbf{0}\\ \mathbf{0} & \boldsymbol{J}_{W_2}^{acc} & \ddots & \vdots\\ \vdots & \ddots & \ddots & \mathbf{0}\\ \mathbf{0} & \cdots & \mathbf{0} & \boldsymbol{J}_{W_k}^{acc}\end{bmatrix}\begin{bmatrix}\boldsymbol{\eta}_1\\ \boldsymbol{\eta}_2\\ \vdots\\ \boldsymbol{\eta}_k\end{bmatrix} + \begin{bmatrix}\mathbf{b}_{W_1}\\ \mathbf{b}_{W_2}\\ \vdots\\ \mathbf{b}_{W_k}\end{bmatrix} \cdots\cdots (20)
$$

$$
\begin{bmatrix}{}^B\ddot{\boldsymbol{p}}_{c_1}\\ {}^B\ddot{\boldsymbol{p}}_{c_2}\\ \vdots\\ {}^B\ddot{\boldsymbol{p}}_{c_k}\end{bmatrix} = \begin{bmatrix}\boldsymbol{J}_{L_1}^{acc} & \mathbf{0} & \cdots & \mathbf{0}\\ \mathbf{0} & \boldsymbol{J}_{L_2}^{acc} & \ddots & \vdots\\ \vdots & \ddots & \ddots & \mathbf{0}\\ \mathbf{0} & \cdots & \mathbf{0} & \boldsymbol{J}_{L_k}^{acc}\end{bmatrix}\begin{bmatrix}\boldsymbol{\eta}_1\\ \boldsymbol{\eta}_2\\ \vdots\\ \boldsymbol{\eta}_k\end{bmatrix} + \begin{bmatrix}\mathbf{b}_{L_1}\\ \mathbf{b}_{L_2}\\ \vdots\\ \mathbf{b}_{L_k}\end{bmatrix} \cdots\cdots (21)
$$

Then, Eqs. (20) and (21) were combined:

$$
\begin{aligned}
\mathbf{0} &= \boldsymbol{J}_B\dot{\boldsymbol{\xi}}_B + \boldsymbol{J}_W^{acc}\boldsymbol{\eta} + \mathbf{b}_W \cdots\cdots (22)\\
\ddot{\boldsymbol{P}}_L &= \boldsymbol{J}_L^{acc}\boldsymbol{\eta} + \mathbf{b}_L \cdots\cdots (23)
\end{aligned}
$$

where $\boldsymbol{J}_B \in \mathbb{R}^{3k\times6}$, $\boldsymbol{J}_W^{acc} \in \mathbb{R}^{3k\times(N+2)k}$, and $\boldsymbol{J}_L^{acc} \in \mathbb{R}^{3k\times(N+2)k}$.

3.2 Inverse Kinematics Considering Priority The angular acceleration of each joint and the constraints on the acceleration level were then obtained by inverse kinematics by considering priority. The inverse kinematics considering priority can be expressed as follows:

$$
\begin{aligned}
\boldsymbol{\eta}^{cmd} &= \boldsymbol{J}_W^{acc\dagger}(-\boldsymbol{J}_B\dot{\boldsymbol{\xi}}_B - \mathbf{b}_W) + (\boldsymbol{I} - \boldsymbol{J}_W^{acc\dagger}\boldsymbol{J}_W^{acc})\boldsymbol{\eta}^{ref}\\
&\qquad\cdots\cdots (24)\\
\boldsymbol{\eta}^{ref} &= \boldsymbol{J}_L^{acc\dagger}(\ddot{\boldsymbol{P}}_L - \mathbf{b}_L) + (\boldsymbol{I} - \boldsymbol{J}_L^{acc\dagger}\boldsymbol{J}_L^{acc})\boldsymbol{u}_{null} \cdots\cdots (25)
\end{aligned}
$$

where $\boldsymbol{J}_W^{acc\dagger}$ and $\boldsymbol{J}_L^{acc\dagger}$ are the pseudo-inverse matrices of $\boldsymbol{J}_W^{acc}$ and $\boldsymbol{J}_L^{acc}$, respectively. Inverse kinematics considering priority realizes a high-priority task using the inverse kinematic solution of the lower-priority task as the null space input for the high-priority task. Then, the low-priority task is realized by the redundancy of the high-priority task. For this robot, the high-priority task is the wheel constraint, and the low-priority task is the leg position constraint. Therefore, the solution of the multiple constraints can be obtained.

4. Problems in Low-Speed Wheeled Locomotion

In this section, a new singular configuration problem in low-speed wheeled locomotion is described. The coefficient vector of $\dot{\gamma}_i$ becomes a zero vector in Eq. (15) when $\dot{\phi}_i = 0$, and vector $\mathbf{a}_{\gamma_i}$ is coaxial to the rotational axis vector $\mathbf{z}_{\gamma_i}$. Thus, $\dot{\gamma}_i^{cmd}$ becomes zero when the wheel is stopped or is rotating at a low speed, causing the steering to vibrate or diverge. This condition is the singular configuration of constraints on the acceleration level. To solve this, the LM method was applied.

4.1 Application of the Levenberg–Marquardt Method The LM method was applied to inverse kinematics considering priority in the acceleration level as a measure of the singular configuration problem in low-speed wheeled locomotion. In the application of the LM method, the pseudo-inverse matrices in Eqs. (24) and (25) are expressed as follows:

$$
\begin{aligned}
\boldsymbol{J}_W^{acc\dagger} &= \boldsymbol{J}_W^{accT}(\boldsymbol{J}_W^{acc}\boldsymbol{J}_W^{accT} + \lambda_W\boldsymbol{I})^{-1} \cdots\cdots (26)\\
\boldsymbol{J}_L^{acc\dagger} &= \boldsymbol{J}_L^{accT}(\boldsymbol{J}_L^{acc}\boldsymbol{J}_L^{accT} + \lambda_L\boldsymbol{I})^{-1} \cdots\cdots (27)
\end{aligned}
$$

Here, the LM method is added to the damping factor in the pseudo-inverse matrix. The inverse kinematic solution does not occur as a local maximum in the singular configuration because the pseudo-inverse matrix becomes the full rank in the case of a rank deficiency in the Jacobian matrix. Therefore, the LM method is able to suppress excessive output in a near-singular configuration.

The damping factor in the LM method greatly affects the calculated result and is thus necessary to determine the combined motion of the robot. Several studies have examined the decision method for the damping factor [29]–[36]. Nakamura *et al.* proposed a method in which a damping factor based on manipulability was added in cases where the manipulability was less than the threshold [30]. Wampler proposed a method of adding a small constant value to the damping factor [20]. Ford *et al.* proposed a method to use the negative natural exponential of the value of the Jacobian matrix determinant as the damping factor and then applied the LM method to the singular configuration of the control moment gyros [31]. Kelmar *et al.* proposed a method for using the current and previous-step manipulability as the damping factor in the LM method of a sequential calculation [32]. Mayorga *et al.* proposed a method that limited the minimum of the singular value of the Jacobian matrix in the damping factor [33]. Sugihara proposed a method that used the square norm of the error and added a small value to the damping factor [34]. Maciejewski *et al.* proposed a method that limited the joint velocity value using the LM method [35]. Deo *et al.* mentioned that Maciejewski's method determines the damping factor within the framework of the trust region method [36]. All these methods can be classified as one of the following:

- Method based on robot manipulability [29]–[33]
- Method based on error minimization [34]–[36]

Methods based on error minimization cannot obtain a suitable damping factor when using inverse kinematics considering priority because the trajectory tracking performance of low-priority tasks is reduced. Therefore, methods based on robot manipulability were applied for the singular configuration problem in the low-speed region, as described in the following subsection. Ford's method [31] was first applied as a conventional method. A method resolving the posture of the steering joint [29] was also applied. Finally, a simpler method

considering the posture of the steering joint was proposed.

4.1.1 Conventional Levenberg–Marquardt Method [31]

Ford *et al*. proposed using the negative natural exponential of the determinant of the Jacobian matrix as the damping factor. By applying this method to the wheel-legged mobile robot, the damping factors in Eqs. (26) and (27) become

$$\lambda_W = \alpha_W e^{-\det(\boldsymbol{J}_W^{acc}\boldsymbol{J}_W^{accT})} \quad \cdots\cdots (28)$$

$$\lambda_L = \alpha_L e^{-\det(\boldsymbol{J}_L^{acc}\boldsymbol{J}_L^{accT})} \quad \cdots\cdots (29)$$

where the values α_W and α_L are empirically obtained.

4.1.2 Method Resolving the Posture of the Steering Joint [29] Because the conventional LM method gives the same damping effect for all the legs, it cannot suppress the vibration associated with each leg's posture. Furthermore, the damping effect is influenced by motion unless the posture is far from the singular configuration. Therefore, the damping factor was altered to reflect the posture of each leg and reduce the damping effects when far from the singular configuration. The damping factors $\lambda_W \boldsymbol{I}, \lambda_L \boldsymbol{I} \in \mathbb{R}^{3k\times 3k}$ are given as follows:

$$\lambda_W \boldsymbol{I} = \begin{bmatrix} \lambda_{W_1} & \boldsymbol{0} & \cdots & \boldsymbol{0} \\ \boldsymbol{0} & \lambda_{W_2} & \ddots & \vdots \\ \vdots & \ddots & \ddots & \boldsymbol{0} \\ \boldsymbol{0} & \cdots & \boldsymbol{0} & \lambda_{W_k} \end{bmatrix} \quad \cdots\cdots (30)$$

$$\lambda_L \boldsymbol{I} = \begin{bmatrix} \lambda_{L_1} & \boldsymbol{0} & \cdots & \boldsymbol{0} \\ \boldsymbol{0} & \lambda_{L_2} & \ddots & \vdots \\ \vdots & \ddots & \ddots & \boldsymbol{0} \\ \boldsymbol{0} & \cdots & \boldsymbol{0} & \lambda_{L_k} \end{bmatrix} \quad \cdots\cdots (31)$$

where

$$\lambda_{W_i} = \alpha_{W_i} e^{-w_{W_i}\beta_{W_i}} \boldsymbol{I}_{dls} \quad \cdots\cdots (32)$$

$$\lambda_{L_i} = \alpha_{L_i} e^{-w_{L_i}\beta_{L_i}} \boldsymbol{I}_{dls} \quad \cdots\cdots (33)$$

$$w_{W_i} = \sqrt{\det(\boldsymbol{J}_{W_i}^{acc}\boldsymbol{J}_{W_i}^{accT})} \quad \cdots\cdots (34)$$

$$w_{L_i} = \sqrt{\det(\boldsymbol{J}_{L_i}^{acc}\boldsymbol{J}_{L_i}^{accT})} \quad \cdots\cdots (35)$$

$\boldsymbol{I}_{dls} \in \mathbb{R}^{3\times 3}$ is the identity matrix, and $\alpha_{W_i}, \alpha_{L_i}, \beta_{W_i}$, and β_{L_i} are scalar parameters. The LM method was applied according to the manipulability of each leg. Therefore, the vibration suppression in the steering joint becomes more effective when the wheel rotates at a low speed or stops completely.

The effective reflection of the steering motion is necessary because the singular configuration of the steering joint affects motion generation. Therefore, the evaluation indexes w_{W_i} and w_{L_i} decompose the manipulability of the steering joint from each leg and are given as

$$w_{W_i} = K_{W_{legi}} \sqrt[3]{\det(\boldsymbol{J}_{legi}\boldsymbol{J}_{legi}^T)} + K_{W\gamma_i}|\det(\boldsymbol{\kappa}_{W\gamma_i}^T\boldsymbol{\kappa}_{W\gamma_i})| \quad \cdots\cdots (36)$$

$$w_{L_i} = K_{L_{legi}} \sqrt[3]{\det(\boldsymbol{J}_{legi}\boldsymbol{J}_{legi}^T)} + K_{L\gamma_i}|\det(\boldsymbol{\kappa}_{L\gamma_i}^T\boldsymbol{\kappa}_{L\gamma_i})| \quad \cdots\cdots (37)$$

$$\boldsymbol{\kappa}_{W\gamma_i} = \dot{\boldsymbol{J}}_{\gamma_i} + {}^w\boldsymbol{\omega}_B^{\wedge}\boldsymbol{J}_{\gamma_i} - \boldsymbol{J}_{\gamma_i}^{\omega\wedge B}\boldsymbol{R}_{c_i}\begin{bmatrix} R\dot{\phi}_i \\ 0 \\ 0 \end{bmatrix} \quad \cdots\cdots (38)$$

$$\boldsymbol{\kappa}_{L\gamma_i} = \dot{\boldsymbol{J}}_{\gamma_i} \quad \cdots\cdots (39)$$

The first term on the right-hand side of Eqs. (36) and (37) is the manipulability of the third joint from the first joint, and the second term is the singular value of the steering joint of each constraint. $K_{W_{legi}}$, $K_{L_{legi}}$, $K_{W_{\gamma_i}}$ and $K_{L\gamma_i}$ are the weighted factors. The singular value of the steering joint expresses the size of the rotational motion of the steering joint. Here, adding each term directly in Eqs. (36) and (37) is not appropriate because their orders are different. In our robot, the first and second terms correspond to three joints and one joint, respectively. Therefore, the orders of each term are different when the square root is calculated in the same way as the general manipulability. Thus, each term changes the identical order based on the number of singular values [37]. From the above, the LM method that considers the influence of the steering joint was applied.

4.1.3 Proposed Method Using a Weighted Matrix

Using a method that resolves the steering joint posture is complicated because it calculates multiple manipulabilites separately. Therefore, a method using a weighted matrix was proposed using the following evaluation:

$$w = \sqrt{\det(\boldsymbol{J}\boldsymbol{W}\boldsymbol{J}^T)} \quad \cdots\cdots (40)$$

where $\boldsymbol{J} \in \mathbb{R}^{m\times n}$ is the Jacobian matrix, $\boldsymbol{W} \in \mathbb{R}^{n\times n}$ is the weighted matrix, and m and n are the degrees of freedom of the workspace and joint space, respectively. Each matrix is given below:

$$\boldsymbol{J} = \begin{bmatrix} j_{11} & \cdots & j_{1(n-1)} & j_{1n} \\ \vdots & \ddots & \vdots & \vdots \\ j_{(m-1)1} & \cdots & j_{(m-1)(n-1)} & j_{(m-1)n} \\ j_{m1} & \cdots & j_{m(n-1)} & j_{mn} \end{bmatrix} \quad \cdots\cdots (41)$$

$$\boldsymbol{W} = \begin{bmatrix} K_1 & 0 & \cdots & 0 \\ 0 & \ddots & \ddots & \vdots \\ \vdots & \ddots & K_{(n-1)} & 0 \\ 0 & \cdots & 0 & K_n \end{bmatrix} \quad \cdots\cdots (42)$$

where j_{mn} is the element of the Jacobian matrix and K_n is the weighted factor of the n^{th} joint. Then, the evaluation indexes w_{W_i}, w_{L_i} on our robot are given as follows:

$$w_{W_i} = \sqrt{\det(\boldsymbol{J}_{W_i}^{acc}\boldsymbol{W}_{W_i}\boldsymbol{J}_{W_i}^{accT})} \quad \cdots\cdots (43)$$

$$w_{L_i} = \sqrt{\det(\boldsymbol{J}_{L_i}^{acc}\boldsymbol{W}_{L_i}\boldsymbol{J}_{L_i}^{accT})} \quad \cdots\cdots (44)$$

where $\boldsymbol{W}_{W_i}$ and $\boldsymbol{W}_{L_i}$ are the weighted matrices defined as

$$\boldsymbol{W}_{W_i} = \begin{bmatrix} K_{W_{legi}} & & & & & \boldsymbol{0} \\ & K_{W_{legi}} & & & & \\ & & K_{W_{legi}} & & & \\ & & & K_{W_{\gamma_i}} & & \\ \boldsymbol{0} & & & & & K_{W_{legi}} \end{bmatrix} \quad \cdots\cdots (45)$$

$$\boldsymbol{W}_{L_i} = \begin{bmatrix} K_{L_{legi}} & & & & & \boldsymbol{0} \\ & K_{L_{legi}} & & & & \\ & & K_{L_{legi}} & & & \\ & & & K_{L\gamma_i} & & \\ \boldsymbol{0} & & & & & K_{L_{legi}} \end{bmatrix} \quad \cdots\cdots (46)$$

Here, the weighted factor of the steering joint is given a different value from the other joints, thus effectively reflecting the steering joint's influence. In addition, this method does not require decomposition of the manipulability beforehand, which is required by the method that resolves the posture of the steering joint. Therefore, the evaluation index does not become complicated.

The evaluation indexes of each method are different; therefore, the evaluation indexes of the conventional LM method and the method for resolving the posture of the steering joint were adjusted by scaling factors. Thus, Eqs. (28) and (29) are modified as follows:

$$\lambda_W = \alpha_W e^{-\frac{\det(\boldsymbol{J}_W^{acc}\boldsymbol{J}_W^{accT})\beta_W}{c_{Wconv}}} \quad \cdots\cdots (47)$$

$$\lambda_L = \alpha_L e^{-\frac{\det(\boldsymbol{J}_L^{acc}\boldsymbol{J}_L^{accT})\beta_L}{c_{Lconv}}} \quad \cdots\cdots (48)$$

where β_W and β_L are scalar parameters and c_{Wconv} and c_{Lconv} are the scaling coefficients given below:

$$c_{Wconv} = \frac{\det(\boldsymbol{J}_W^{acc}\boldsymbol{J}_W^{accT})}{\sqrt{\det(\boldsymbol{J}_{W_i}^{acc}\boldsymbol{W}_{W_i}\boldsymbol{J}_{W_i}^{accT})}} \quad \cdots\cdots (49)$$

$$c_{Lconv} = \frac{\det(\boldsymbol{J}_L^{acc}\boldsymbol{J}_L^{accT})}{\sqrt{\det(\boldsymbol{J}_{L_i}^{acc}\boldsymbol{W}_{L_i}\boldsymbol{J}_{L_i}^{accT})}} \quad \cdots\cdots (50)$$

The scaling coefficient is the evaluation index divided by the evaluation index of the proposed method using the weighted matrix. Here, the evaluation index of each method in the initial posture that had been calculated in advance was used. Similarly, Eqs. (32) and (33) were modified as shown below:

$$\boldsymbol{\lambda}_{W_i} = \alpha_{W_i} e^{-\frac{w_{W_i}\beta_{W_i}}{c_{W_i}}} \boldsymbol{I}_{dls} \quad \cdots\cdots (51)$$

$$\boldsymbol{\lambda}_{L_i} = \alpha_{L_i} e^{-\frac{w_{L_i}\beta_{L_i}}{c_{L_i}}} \boldsymbol{I}_{dls} \quad \cdots\cdots (52)$$

where c_{W_i} and c_{L_i} are the scaling coefficients, defined as:

$$c_{W_i} = \frac{K_{W_{legi}}\sqrt[3]{\det(\boldsymbol{J}_{legi}\boldsymbol{J}_{legi}^T)} + K_{W\gamma_i}|\det(\boldsymbol{\kappa}_{W\gamma_i}^T\boldsymbol{\kappa}_{W\gamma_i})|}{\sqrt{\det(\boldsymbol{J}_{W_i}^{acc}\boldsymbol{W}_{W_i}\boldsymbol{J}_{W_i}^{accT})}} \quad \cdots\cdots (53)$$

$$c_{L_i} = \frac{K_{L_{legi}}\sqrt[3]{\det(\boldsymbol{J}_{legi}\boldsymbol{J}_{legi}^T)} + K_{L\gamma_i}|\det(\boldsymbol{\kappa}_{L\gamma_i}^T\boldsymbol{\kappa}_{L\gamma_i})|}{\sqrt{\det(\boldsymbol{J}_{L_i}^{acc}\boldsymbol{W}_{L_i}\boldsymbol{J}_{L_i}^{accT})}} \quad \cdots\cdots (54)$$

This scaling coefficient is also the evaluation index divided by the evaluation index of the proposed method using the weighted matrix, and using the evaluation index of each method in the initial posture that had been calculated in advance.

5. Simulation and Experimental Results

A three-dimensional simulation and an experiment considering the singular configuration problem in low-speed wheeled locomotion were performed to verify the proposed method's ability to generate motion.

5.1 Workspace Controller The reference value of the position of each leg and the position of the base link are given below:

$${}^w\ddot{\boldsymbol{p}}_B^{ref} = \boldsymbol{k}_{pB}({}^w\boldsymbol{p}_B^{cmd} - {}^w\boldsymbol{p}_B^{res}) + \boldsymbol{k}_{dB}({}^w\dot{\boldsymbol{p}}_B^{cmd} - {}^w\dot{\boldsymbol{p}}_B^{res}) \quad \cdots\cdots (55)$$

$${}^B\ddot{\boldsymbol{p}}_{c_i}^{ref} = \boldsymbol{k}_{pc_i}({}^B\boldsymbol{p}_{c_i}^{cmd} - {}^w\boldsymbol{p}_{c_i}^{res}) + \boldsymbol{k}_{dc_i}({}^B\dot{\boldsymbol{p}}_{c_i}^{cmd} - {}^B\dot{\boldsymbol{p}}_{c_i}^{res}) \quad \cdots\cdots (56)$$

$${}^w\dot{\boldsymbol{\omega}}_B^{ref} = \boldsymbol{T}(\boldsymbol{\Phi})\ddot{\boldsymbol{\Phi}}^{ref} \quad \cdots\cdots (57)$$

$$\ddot{\boldsymbol{\Phi}}^{ref} = \boldsymbol{k}_{p\Phi}(\boldsymbol{\Phi}^{cmd} - \boldsymbol{\Phi}^{res}) + \boldsymbol{k}_{d\Phi}(\dot{\boldsymbol{\Phi}}^{cmd} - \dot{\boldsymbol{\Phi}}^{res}) \quad \cdots\cdots (58)$$

where $\boldsymbol{T}(\boldsymbol{\Phi})$ is the transformation matrix between ${}^w\dot{\boldsymbol{\omega}}_B^{ref}$ and $\dot{\boldsymbol{\Phi}}$. The relationship between ${}^w\dot{\boldsymbol{\omega}}_B^{ref}$ and $\dot{\boldsymbol{\Phi}}$ is given by ${}^w\dot{\boldsymbol{\omega}}_B^{ref} = \boldsymbol{T}(\boldsymbol{\Phi})\ddot{\boldsymbol{\Phi}}^{ref} + \dot{\boldsymbol{T}}(\boldsymbol{\Phi})\dot{\boldsymbol{\Phi}}^{ref}$. Here, $\dot{\boldsymbol{T}}(\boldsymbol{\Phi}) \simeq 0$ was assumed because of the low effectiveness of $\dot{\boldsymbol{T}}(\boldsymbol{\Phi})$. The proportion and derivative gains are $\boldsymbol{k}_{pB}$, $\boldsymbol{k}_{pc_i}$, and $\boldsymbol{k}_{p\Phi}$ and $\boldsymbol{k}_{dB}$, $\boldsymbol{k}_{dc_i}$, and $\boldsymbol{k}_{d\Phi}$, respectively.

Next, joints other than the steering joint were controlled by the acceleration control and the disturbance observer [38]; their torque is given as

$$\boldsymbol{\tau}_{\theta_i,\phi_i}^{ref} = \boldsymbol{M}_n\ddot{\boldsymbol{\eta}}_{\theta_i,\phi_i}^{ref} + \hat{\boldsymbol{\tau}}_{\theta_i,\phi_i}^{dis} \quad \cdots\cdots (59)$$

where $\boldsymbol{M}_n$ is the diagonal matrix related to the nominal inertia of each joint other than the steering joint and $\hat{\boldsymbol{\tau}}_{\theta_i,\phi_i}^{dis}$ is the estimated disturbance torque by the disturbance observer. The angular acceleration reference $\ddot{\boldsymbol{\eta}}_{\theta_i,\phi_i}^{ref}$ is then

$$\ddot{\boldsymbol{\eta}}_{\theta_i,\phi_i}^{ref} = \ddot{\boldsymbol{\eta}}_{\theta_i,\phi_i}^{cmd} + \boldsymbol{k}_{p\theta_i,\phi_i}(\boldsymbol{\eta}_{\theta_i,\phi_i}^{cmd} - \boldsymbol{\eta}_{\theta_i,\phi_i}^{res}) + \boldsymbol{k}_{d\theta_i,\phi_i}(\dot{\boldsymbol{\eta}}_{\theta_i,\phi_i}^{cmd} - \dot{\boldsymbol{\eta}}_{\theta_i,\phi_i}^{res}) \quad \cdots\cdots (60)$$

where $\boldsymbol{k}_{p\theta_i,\phi_i}$ and $\boldsymbol{k}_{d\theta_i,\phi_i}$ are the proportional and derivative gains, respectively. Furthermore, the steering joint was controlled by the proportional control and the disturbance observer. The torque reference of the steering joint is given as

$$\tau_{\gamma_i}^{ref} = k_{p\gamma_i}(\dot{\gamma}_i^{cmd} - \dot{\gamma}_i^{res}) + \hat{\tau}_{\gamma_i}^{dis} \quad \cdots\cdots (61)$$

where $k_{p\gamma_i}$ is the proportional gain and $\hat{\tau}_{\gamma_i}^{dis}$ is the estimated disturbance torque of the steering joint by the disturbance observer. A block diagram of the entire control system is shown in Fig. 4.

5.2 Simulation Results The behavior of the robot was confirmed in case of the posture of the singular configuration and the nonsingular configuration as shown in Fig. 5. Figure 5(a) is the singular configuration because the steering joint is perpendicular to the contact point. By contrast, Fig. 5(b) is not perpendicular to the contact point, therefore, this posture is the nonsingular configuration. The constant velocity trajectory was given to $\boldsymbol{\Phi}$, ${}^w\boldsymbol{p}_B(= [x_B\ y_B\ z_B]^T)$, and ${}^B\boldsymbol{p}_{c_i}(= [x_{c_i}\ y_{c_i}\ z_{c_i}]^T)$. As shown in Fig. 5, the given target trajectory was 0.1 m/s in the x-direction when the singular configuration and 0.5 m/s in the y-direction when the nonsingular configuration. The weighted factors used in the method resolving the posture of the steering joint and the proposed method are given in Table 1. The scalar parameters in each method are given in Table 2, and the same values were used for all the methods. Here, each weighted factor and scalar parameter were experimentally determined. The

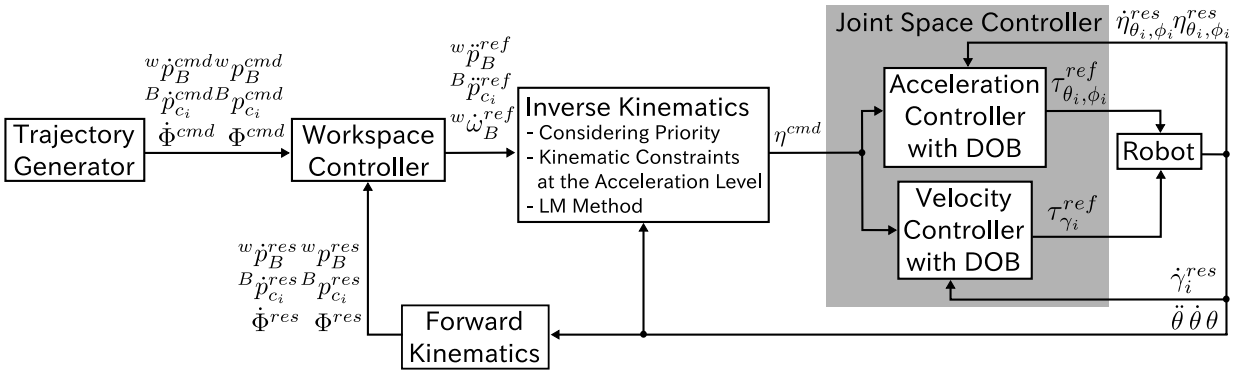

Fig. 4. Control system block diagram (DOB: disturbance observer)

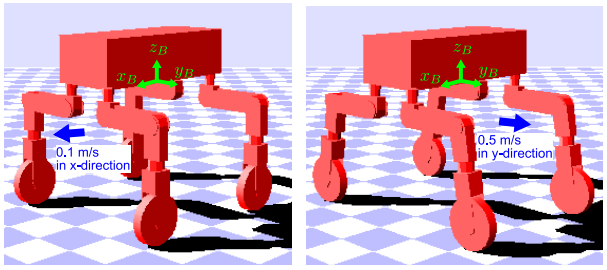

(a) Condition of the singular configuration (b) Condition of the nonsingular configuration

Fig. 5. Condition of the posture in the simulation

Table 1. Weighted factor conditions

Contents	$K_{W_{legi}}$	$K_{W_{\gamma_i}}$	$K_{L_{legi}}$	$K_{L_{\gamma_i}}$
Simulation	1.00	50.0	1.00	0.50
Experiment	1.00	50.0	1.00	0.50

Table 2. Scalar parameter conditions

Contents	α_W	α_L	β_W	β_L	α_{W_i}	α_{L_i}	β_{W_i}	β_{L_i}
Simulation	0.01	1.45	150.0	50.0	0.01	1.45	150.0	50.0
Experiment	1.50	0.014	250.0	100.0	1.50	0.014	250.0	100.0

simulation was performed using the robot control simulator (ROCOS) [39].

The simulation results of the singular configuration are first described. The base position-tracking trajectory in the x-direction and the steering angle of the first leg are shown in Figs. 6 and 7. Figure 6 presents the results when a single kinematic constraint on the acceleration level is used, and Fig. 7 presents the results when the conventional LM method, the method that resolves the posture of the steering joint, and the proposed method using the weighted matrix are used. The standard deviation of the steering angle and the root mean square errors (RMSEs) of the base position-tracking trajectory are given in Table 3. As shown in Fig. 6(a), steering vibration occurred at the start of motion, near the singular configuration. Furthermore, a base position-tracking error occurred at the beginning of motion, as shown in Fig. 6(b). This tracking error was caused by vibration in the steering joint. Figure 7 shows the effective vibration suppression and base position tracking realized in each LM method. From Table 3, each LM method has almost the same effect regarding the tracking of the base position. In addition, the proposed method using the weighted matrix was most effective in vibration suppression of the steering joint. Therefore, the proposed method using the weighted matrix effectively reflects the influence of the steering joint.

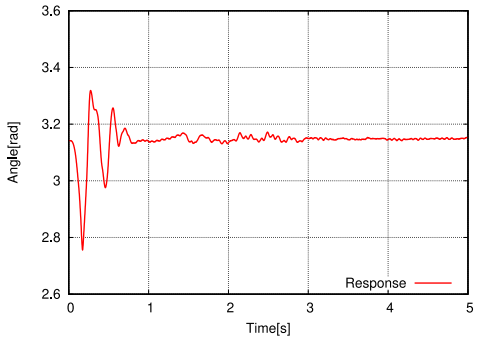

(a) Response of the steering angle

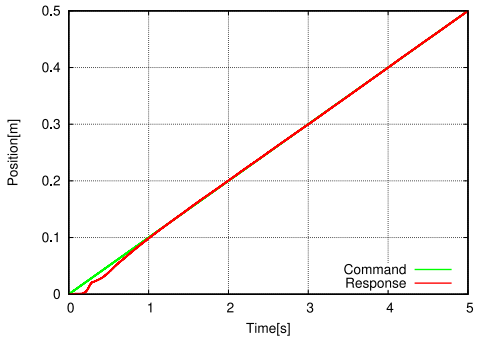

(b) Response of the base position

Fig. 6. Simulation results using a single kinematic constraint on the acceleration level in the case of the singular configuration

The simulation results of the nonsingular configuration are described. Figures 8 and 9 show the base position-tracking trajectory in the y-direction and the steering angle of the first leg. The results with a single kinematic constraint on the acceleration level is shown in Fig. 8. The results of the conventional LM method, the method that resolves the posture of the steering joint, and the proposed method using the weighted matrix are shown in Fig. 9. Table 4 shows the standard deviation of the steering angle and the RMSEs of the base position-tracking trajectory. From the result of a single kinematic constraint on the acceleration level in Fig. 8, the steering joint did not vibrate and the base position-tracking error was small since the posture is the nonsingular configuration. From Fig. 9, the steering vibration and the base position-tracking error occurred in the conventional LM method because the

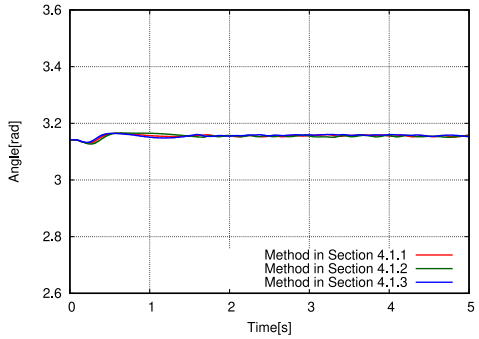

(a) Response of the steering angle

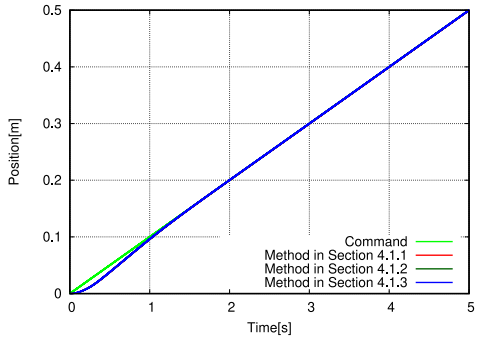

(b) Response of the base position

Fig. 7. Simulation results using the LM method in the case of the singular configuration

Table 3. Standard deviation of the steering angle and RMSEs of the base link in the simulation results of the nonsingular configuration

Contents	SD[mrad]	RMSEs[mm]
Single kinematic constraint on the acceleration level	51.455	2.414
Conventional LM method	5.909	2.671
Method resolving the posture of the steering joint	7.163	2.629
Proposed method using the weighted matrix	5.849	2.642

Table 4. Standard deviation of the steering angle and RMSEs of the base link in the simulation results of the nonsingular configuration

Contents	SD[mrad]	RMSEs[mm]
Single kinematic constraint on the acceleration level	0.884	14.780
Conventional LM method	16.274	73.183
Method resolving the posture of the steering joint	8.385	16.441
Proposed method using the weighted matrix	1.689	16.667

effect of the damping factor was not sufficiently decreased. In the method resolving the posture of the steering joint, the steering vibration occurred, however, the base-position tracking error was small. In addition, the steering vibration and the base position-tracking error of the proposed method using the weighted matrix were small. From Table 4, the steering vibration and the base position-tracking error in the case of a single kinematic constraint on the acceleration level were smaller than the LM methods. The proposed method using the weighted matrix was realized the base position-tracking error almost the same as the case of a single kinematic constraint on the acceleration level. Then, the steering vibration of the proposed method using the weighted matrix was smaller than the other LM method and was sufficiently small in the realization of the motion. Therefore, the proposed method using the weighted matrix can be realized the effective motion generation even in the nonsingular configuration.

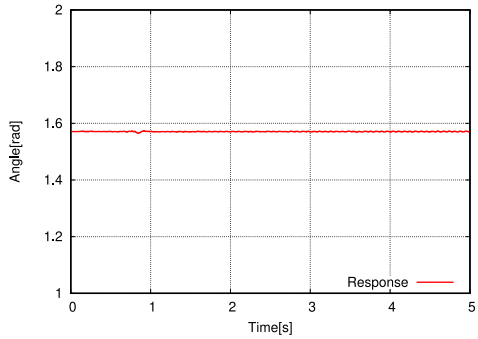

(a) Response of the steering angle

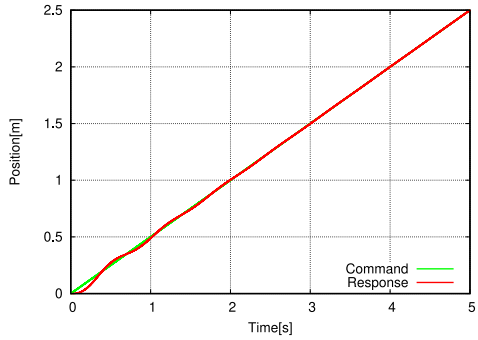

(b) Response of the base position

Fig. 8. Simulation results using a single kinematic constraint on the acceleration level in the case of the nonsingular configuration

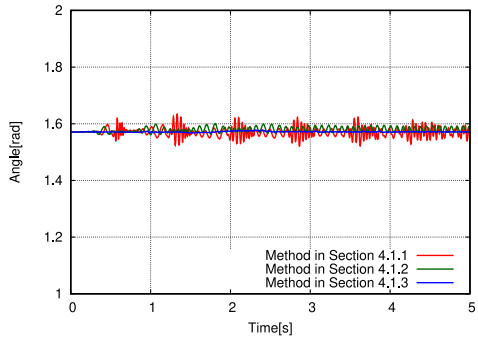

(a) Response of the steering angle

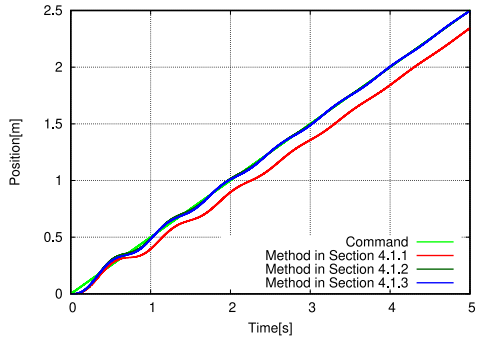

(b) Response of the base position

Fig. 9. Simulation results using the LM method in the case of the nonsingular configuration

5.3 Experimental Results The experimental results confirmed the simulation results presented in the previous section. Here, the verification was performed for the case of the singular configuration. The LM methods that considered the scaling coefficients were used. In addition, the weighted

factors and the scalar parameters are given in Tables 1 and 2, respectively. Next, the motion sequence of the experiment is shown in Fig. 10. To achieve the same posture as the simulation, a base link trajectory that rises 0.104 m in the z-direction over 4.0 s was first given. A trajectory moving 0.40 m in the x-direction for 4.0 s was also given. Finally, a trajectory that descends 0.104 m in the z-direction over 4.0 s was given to return to the initial posture.

The experimental results of the conventional LM method, the method of resolving the posture of the steering joint, and the proposed method using the weighted matrix are shown in Figs. 11, 12, and 13, respectively. Each figure shows the position of the base link, the steering joints angle, and the damping factors of the wheel and leg position constraints. The standard deviations of the steering angle of the first leg and the RMSEs of the base position-tracking trajectory are given in Table 5. From Fig. 11, the conventional LM method was an emergency stop because the steering joint was rotated for around 6.0 s. The damping factor changed drastically from around 3.0 s and affected the steering joint. Therefore, it was impossible to realize the motion. From Figs. 12 and 13, the method resolving the posture of the steering joint and the proposed method using the weighted matrix realized a trajectory tracking motion of the base link. In addition, with the proposed method using the weighted matrix, the standard deviation of the steering angle was reduced to 49.5% of the method resolving the posture of the steering joint, as shown in Table 5.

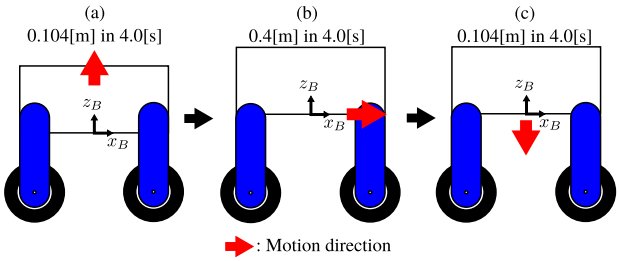

Fig. 10. Motion sequence of the experiment: (a) base link rises 0.104 m in 4.0 s; (b) robot moves 0.4 m in 4.0 s; and (c) base link descends 0.104 m in 4.0 s

5.4 Discussion Here, we discuss the above results and the effect of each LM method. From the result of the conventional LM method in Fig. 11, the damping factor changed drastically, which affected the motion of the steering joint. The change in the damping factor occurred because the manipulability of the whole body was decreased. However, the method resolving the posture of the steering joint and the proposed method using the weighted matrix prevented the damping factor from increasing because the evaluation index

Table 5. Standard deviation of the steering angle and RMSEs of the base link in the experimental results

Contents	SD[mrad]	RMSEs[mm]
Conventional LM method	—	—
Method resolving the posture of the steering joint	15.614	1.895
Proposed method using the weighted matrix	7.729	1.821

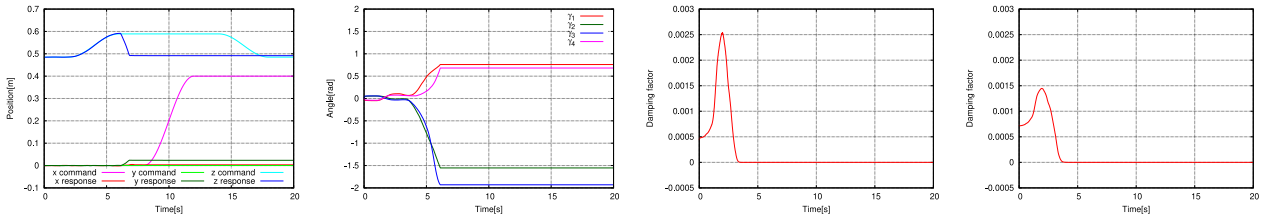

(a) Response of the base position (b) Response of the steering angle (c) Damping factor of constraint of the wheel (d) Damping factor of constraint of the leg position

Fig. 11. Experimental results using the conventional LM method

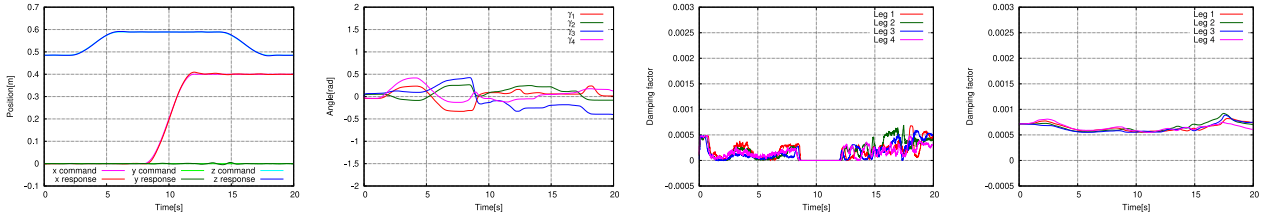

(a) Response of the base position (b) Response of the steering angle (c) Damping factor of constraint of the wheel (d) Damping factor of constraint of the leg position

Fig. 12. Experimental results using the method of resolving the posture of the steering joint

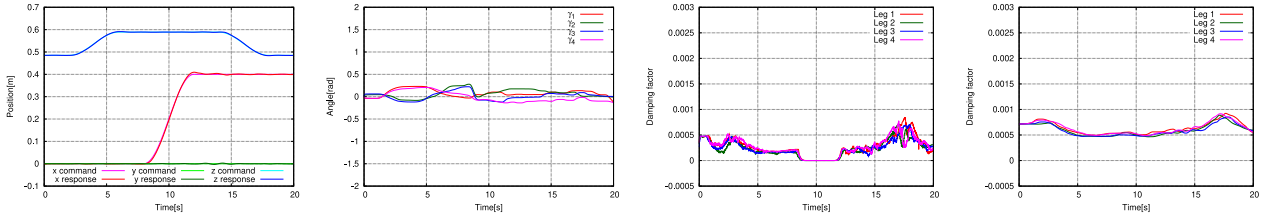

(a) Response of the base position (b) Response of the steering angle (c) Damping factor of constraint of the wheel (d) Damping factor of constraint of the leg position

Fig. 13. Experimental results using the proposed method with a weighted matrix

Table 6. Computational time of each method

Contents	Time[μs]
Conventional LM method	8.168
Method resolving the posture of the steering joint	5.124
Proposed method using the weighted matrix	6.968

was calculated by each leg. Next, from Table 5, the standard deviation of the steering angle was smaller in the proposed method using the weighted matrix than in the method resolving the posture of the steering joint. The damping factor of the method resolving the posture of the steering joint, shown in Fig. 12, changed considerably by the start of motion and became small. In contrast, for the proposed method using the weighted matrix shown in Fig. 13, it changed slowly with the start of motion. Furthermore, Eqs. (36) and (37) of the method resolving the posture of the steering joint separated the target joint and ignored part of the influence of the target joint. Then, Eqs. (43) and (44) of the proposed method using the weighted matrix reflected all the influences of the target joint because the weighting is given by the weighted matrix. Therefore, the proposed method using the weighted matrix considered all the influences on the target joint and realized the generation of effective motion. Finally, the computational cost of each method became $O(l^3)$. Here, l is the matrix size and is dependent on the Jacobian matrix. The computational time of each method in the experiment is given in Table 6: the method resolving the posture of the steering joint was the quickest because the size of the matrix is the smallest. However, the computational times of each method are almost the same because they are of the order of microseconds. From the above, the proposed method using the weighted matrix does not need to separate the target joint in advance unlike the method resolving the posture of the steering joint, and the generation of effective motion can be realized.

6. Conclusion

A method using inverse kinematics that considers priority and kinematic constraints extended to the acceleration level was applied to the inverse kinematic calculation in the generation of motion for a wheel-legged mobile robot. Motion generation was realized using the redundancy of the robot. Furthermore, a new singular configuration occurring at low-speed wheeled locomotion was identified in the acceleration level. The LM method was applied to this problem. A method for determining the damping factor using a weighted matrix to reflect the influence of the steering joint was then proposed. The effectiveness of the proposed method was verified by a three-dimensional simulation and experiment. The results show that the wheel-legged mobile robot was able to generate motion in the singular configuration using the proposed method. Moreover, the proposed damping factor of the LM method achieved effective trajectory tracking and generated motion of the steering joint by a simple approach.

References

(1) T. Yoshioka, T. Takubo, T. Arai, and K. Inoue: “Hybrid locomotion of leg-wheel ASTERISK H”, *J. Robotics and Mechatronics*, Vol.20, No.3, pp.403–412 (2008)

(2) B.H. Wilcox: “ATHLETE: A cargo and habitat transporter for the moon”, Proc. IEEE Aerospace Conference, pp.1–7 (2009)

(3) T. Thomson, I. Sharf, and B. Beckman: “Kinematic control and posture optimization of a redundantly actuated quadruped robot”, Proc. IEEE Int. Conf. on Robotics and Automation, pp.1895–1900 (2012)

(4) N. Koyachi, K. Maruyama, Y. Kawai, F. Tomita, and Y. Morikawa: “Step over motion of four wheeled and four legged flexible personal robot”, Proc. IEEE Int. Conf. on Robotics and Biomimetics, pp.616–621 (2009)

(5) D. Leidner, A. Dietrich, M. Beetz, and A. Albu-Schäffer: “Knowledge-enabled parameterization of whole-body control strategies for compliant service robots”, *Autonomous Robots*, Vol.40, No.3, pp.519–536 (2016)

(6) S. Nakajima: “A New Personal Mobility Vehicle for Daily Life: Improvements on a New RT-Mover that Enable Greater Mobility are Showcased at the Cybathlon”, *IEEE Robotics Automation Magazine*, Vol.24, No.4, pp.37–48 (2017)

(7) J.P. Trevelyan, P.D. Kovesi, M. Ong, and D. Elford: “ET: A Wrist Mechanism without Singular Positions”, *Int. J. of Robotics Research*, Vol.4, No.4, pp.71–85 (1986)

(8) V. Milenkovic: “Non-singular industrial robot wrist”, US 4907937, 1990–03–13.

(9) J. Kim, G. Marani, W.K. Chung, and J. Yuh: “Task reconstruction method for real-time singularity avoidance for robotic manipulators”, *Advanced Robotics*, Vol.20, No.4, pp.453–481 (2006)

(10) J.E. Lloyd and V. Hayward: “Singularity-robust trajectory generation”, *Int. J. of Robotics Research*, Vol.20, No.1, pp.38–56 (2001)

(11) U. Pattacini, F. Nori, L. Natale, G. Metta, and G. Sandini: “An experimental evaluation of a novel minimum-jerk cartesian controller for humanoid robots”, Proc. IEEE/RSJ Int. Conf. on Intelligent Robots and Systems, pp.1668–1674 (2010)

(12) Y. Nakamura, H. Hanfusa, and T. Yoshikawa: “Task priority based redundancy control of robot manipulators”, *Int. J. of Robotics Research*, Vol.6, No.2, pp.3–15 (1987)

(13) F.T. Cheng, J.S. Chen, and F.C. Kung: “Study and resolution of singularities for a 7-DOF redundant manipulator”, *IEEE Trans. on Industrial Electronics*, Vol.45, No.3, pp.469–480 (1998)

(14) Z. Kemény: “Redundancy resolution in robots using parameterization through null space”, *IEEE Trans. on Industrial Electronics*, Vol.50, No.4, pp.777–783 (2003)

(15) M. Shimizu, H. Kakuya, W.K. Yoon, K. Kitagaki, and K. Kosuge: “Analytical inverse kinematic computation for 7-DOF redundant manipulators with joint limits and its application to redundancy resolution”, *IEEE Trans. on Robotics*, Vol.24, No.5, pp.1131–1142 (2008)

(16) E. Sariyildiz and H. Temeltas: “Solution of inverse kinematic problem for serial robot using dual quaterninons and plücker coordinates”, Proc. IEEE/ASME Int. Conf. on Advanced Intelligent Mechatronics, pp.338–343 (2009)

(17) S.R. Lucas, C.R. Tischler, and A.E. Samuel: “Real-time solution of the inverse kinematic-rate problem”, *Int. J. of Robotics Research*, Vol.19, No.12, pp.1236–1244 (2000)

(18) T. Kishimoto and Y. Fujimoto: “Numerically stable inverse kinematics calculation of robot manipulators even in singular configuration”, Proc. IEEE Int. Conf. on Industrial Electronics, Control, and Instrumentation, pp.1036–1040 (2004)

(19) D.N. Nenchev, Y. Tsumaki, and M. Uchiyama: “Singularity-consistent behavior of telerobots: Theory and experiments”, *Int. J. of Robotics Research*, Vol.17, No.2, pp.138–152 (1998)

(20) C.W. Wampler: “Manipulator inverse kinematic solutions based on vector formulations and damped least-squares methods”, *IEEE Trans. on Systems, Man, and Cybernetics*, Vol.16, No.1, pp.93–101 (1986)

(21) Y. Xia and J. Wang: “A dual neural network for kinematic control of redundant robot manipulators”, *IEEE Trans. on Systems, Man, and Cybernetics*, Vol.31, No.1, pp.147–154 (2001)

(22) C. Grand, F. Benamar, and F. Plumet: “Motion kinematics analysis of wheeled-legged rover over 3D surface with posture adaptation”, *Int. J. of Mechanism and Machine Theory*, Vol.45, No.3, pp.477–495 (2010)

(23) S.I. An and D.S. Kwon: “Design and kinematic analysis of a 6DOFs omnidirectional mobile robot for the gesture expression”, Proc. ICROS-SICE Int. Joint Conf., pp.129–133 (2009)

(24) A. Suzumura and Y. Fujimoto: “High mobility control for a wheel-legged mobile robot based on resolved momentum control”, Proc. IEEE Int. Workshop on Advanced Motion Control, pp.1–6 (2012)

(25) A. Suzumura and Y. Fujimoto: “Workspace control of a wheel-legged mobile robot for gyrating locomotion with movable leg”, Proc. IEEE Int. Conf. on Mechatronics, pp.641–647 (2013)

(26) K. Levenberg: “A method for the solution of certain non-linear problems in least squares”, *Quarterly of Applied Mathematics*, Vol.2, No.2, pp.164–168 (1944)

(27) D.W. Marquardt: “An algorithm for least-squares estimation of nonlinear parameters”, *J. of the Society for Industrial and Applied Mathematics*, Vol.11, No.2, pp.431–441 (1963)
(28) T. Yoshikawa: “Manipulability of robotic mechanisms”, *Int. J. of Robotics Research*, Vol.4, No.2, pp.3–9 (1985)
(29) K. Nagano and Y. Fujimoto: “Comparison of methods for solving the singular configuration of a wheel-legged mobile robot”, *IEEJ Journal of Industry Applications*, Vol.5, No.5, pp.378–391 (2016)
(30) Y. Nakamura and H. Hanafusa: “Inverse kinematic solutions with singularity robustness for robot manipulator control”, *J. of Dynamic Systems, Measurement, and Control*, Vol.108, No.3, pp.163–171 (1986)
(31) K.A. Ford and C.D. Hall: “Singular direction avoidance steering for control-moment gyros”, *J. of Guidance, Control, and Dynamics*, Vol.23, No.4, pp.648–656 (2000)
(32) L. Kelmar and P.K. Khosla: “Automatic generation of kinematics for a reconfigurable modular manipulator system”, Proc. IEEE Int. Conf. on Robotics and Automation, pp.24–29 (1988)
(33) R.V. Mayorga, A.K.C. Wong, and N. Milano: “A fast procedure for manipulator inverse kinematics evaluation and pseudoinverse robustness”, *IEEE Trans. on Systems, Man, and Cybernetics*, Vol.22, No.4, pp.790–798 (1992)
(34) T. Sugihara: “Solvability-unconcerned inverse kinematics by the Levenberg-Marquardt method”, *IEEE Trans. on Robotics*, Vol.27, No.5, pp.984–991 (2011)
(35) A.A. Maciejewski and C.A. Klein: “The singular value decomposition: Computation and applications to robotics”, *Int. J. of Robotics Research*, Vol.8, No.6, pp.63–79 (1989)
(36) A.S. Deo and I.D. Walker: “Robot subtask performance with singularity robustness using optimal damped least-squares”, Proc. IEEE Int. Conf. on Robotics and Automation, pp.434–441 (1992)
(37) J.O. Kim and P.K. Khosla: “Dexterity measures for design and control of manipulators”, Proc. IEEE/RSJ Int. Workshop on Intelligent Robots and Systems, Vol.2, pp.758–763 (1991)
(38) K. Ohnishi, M. Shibata, and T. Murakami: “Motion control for advanced mechatronics”, *IEEE/ASME Trans. on Mechatronics*, Vol.1, No.1, pp.56–67 (1996)
(39) Y. Fujimoto and A. Kawamura: “Simulation of an autonomous biped walking robot including environmental force interaction”, *IEEE Robotics and Automation Magazine*, Vol.5, No.2, pp.33–42 (1998)

Kenta Nagano (Member) received a B.E. degree in symbiotic systems science from Fukushima University in Fukushima, Japan, in 2013 and M.E. and Ph.D. degrees in electrical and computer engineering from Yokohama National University in Yokohama, Japan, in 2015 and 2018, respectively. His research interests include robotics, mechatronics, and motion control. He is a member of IEE Japan, IEEE, and the Robotics Society of Japan.

Yasutaka Fujimoto (Senior Member) received B.E., M.E., and Ph.D. degrees in electrical and computer engineering from Yokohama National University, Yokohama, Japan, in 1993, 1995, and 1998, respectively. In 1998, he joined the Department of Electrical Engineering at Keio University in Yokohama, Japan, as a research associate. Since 1999, he has been with the Department of Electrical and Computer Engineering at Yokohama National University in Japan, where he is currently a professor. His research interests include motion control and actuators, in particular, the modeling and control of mobile/legged robots and direct-drive actuators with high-thrust force density and high back-drivability. He is a senior member of IEEE and a member of the Robotics Society of Japan, SICE, JSAE, IEICE, and INFORMS.